Sensitivity Analysis of Radiometric and Polarimetric Properties from Simulated Ice Clouds of IR and Sub-mm/mm Bands

James Coy[1], Adam Bell[1], Guanglin Tang[1], Ping Yang[1] and Dong L. Wu[2]

[1]Department of Atmospheric Sciences, Texas A&M University, College Station, TX
[2]Climate and Radiation Lab, NASA Goddard Space Flight Center, Greenbelt, MD

ATMOSPHERIC SCIENCES
TEXAS A&M UNIVERSITY

Abstract

Radiometric and polarimetric calculations of simulated ice clouds composed entirely of aggregate particles are conducted for several wavelengths in the Infrared (IR) and Sub-millimeter/Millimeter (Sub-mm/mm) ranges as part of NASA's SWIRP (Compact Submm-Wave and LWIR Polarimeters for Cirrus Ice Properties) project. In this study, the scattering/absorption/polarization properties of the aggregates that were calculated at the selected bands before this study are incorporated into a radiative transfer model, ARTS (Atmospheric Radiative Transfer Model) in order to explore ice cloud characteristics in 1D spherical atmospheres and the possibility of retrieving ice water paths (IWPs) and effective diameters (D_{eff}s) using the selected Sub-mm/mm and IR wavelengths.

This study focuses on simulating cirrus clouds using the wavelengths of 441 μm (680 GHz), 1363 μm (220 GHz), 8.6 μm, 11 μm, and 12 μm. The simulated cirrus clouds are made to be composed of a single ice particle habit of 8-column aggregates with a gamma distribution of particle sizes. Simulations are performed for combinations of IWPs, D_{eff}s, visible optical thicknesses (τ), and certain viewing zenith angles (θ) with ambient temperatures and pressure levels corresponding to a typical tropical atmosphere. The sensitivity analyses for these cases will focus on the creation of plots that display isolines of IWP and D_{eff} with brightness temperature parameters representing the axes for a combination of 2-3 wavelengths. The brightness temperature parameters being used for this study are polarization difference (PD) for microwave wavelengths, brightness temperature depression from a cloud-free atmosphere (ΔT_b), and IR split-window brightness temperature differences (BTDs) that are based on the computed radiances from the ARTS calculations.

Simulation Methodology

The Atmospheric Radiative Transfer Simulator (ARTS)

- Simulations done for this study were performed by a fully polarized forward model known as the Atmospheric Radiative Transfer Simulator (ARTS) version 2.
- Can perform simulations for 1D, 2D, and 3D atmospheres and allows users to modify atmospheric parameters such as temperature and pressure levels specific to their situation.
- ARTS also allows for the simple insertion of simulated clouds known as a "cloud box" by specifying the height/pressure levels they should be placed in.
- Can solve the scattering portion of the radiative transfer equation by using two methods known as the backward Monte Carlo method and the Discrete Ordinate Iterative Method (DOIT) method.
  - A 1D atmosphere (Figure 1) was chosen to be used in this study which the use of the DOIT method is recommended.
  - The DOIT method solves the radiative transfer equation by restricting the scattering portion to be done only inside the cloud box to reduce computation time (Emde et al. 2004).

Figure 1: Schematic of a 1D atmosphere implemented in ARTS with a cloud box. The radius of the ellipsoid, the surface and all pressure levels are constant around the globe (Buehler et al. 2017).

Simulation Settings

- Sensor located at an altitude of 950 km (Sub-mm/mm channels) and 2000 km (IR channels) with viewing zenith angles (θ) at nadir (0°) and 55°.
- **Wavelengths used:**
  - **441 μm (680 GHz) and 1363 μm (220 GHz) (Sub-mm/mm Microwave channels).**
  - **8.6 μm, 11 μm, and 12 μm (Infrared channels).**
- Cloud Box:
  - Cases corresponding to high-altitude cirrus clouds.
  - Layer at 300 hPa to 250 hPa.
  - Composed of randomly oriented 8-column aggregate ice particles with single scattering properties from the MODIS Collection 6 (MC6) product.
  - **Ice Water Paths (IWPs) ranging from $10\ gm^{-2}$ to $200\ gm^{-2}$.**
    - **$10, 20, 30, 40, 50, 60, 70, 80, 90, 100, 120, 140, 160, 180, 200\ gm^{-2}$.**
  - **Ice particle sizes under a Gamma distribution with effective diameters (D_{eff}) ranging from 10 μm to 100 μm.**
    - **$10, 20, 30, 40, 50, 60, 70, 80, 90, 100$ μm.**
  - Simulated atmosphere composed of pressure and temperature corresponding to a typical tropical atmosphere (Figure 2).

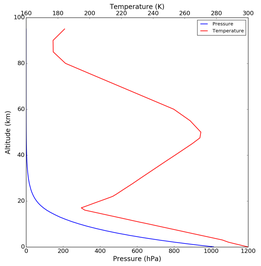

Figure 2: Pressure (bottom x-axis) and temperature (top x-axis) profiles used by ARTS to simulate an atmosphere similar to what is typically observed in a tropical atmosphere.

Sub-mm/mm Polarization Difference (PD) Sensitivity

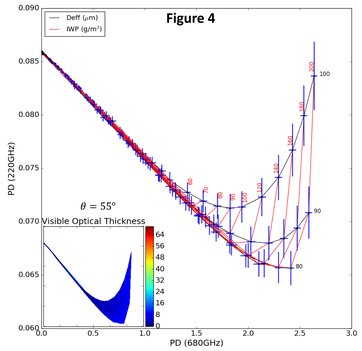

Figure 4: IWP (red) and D_{eff} (black) isoline plot of PDs with respect to 680 GHz and 220 GHz. The potential error lines (blue) are centered at all intercepts of the IWP and D_{eff} isolines. The visible optical thickness (τ) contour subplot contains axes of the same scale as the main plot. The viewing zenith angle (θ) is 55°.

(1) $T_{bv} = T_b(I + Q)$ (Vertically Polarized Brightness Temperature)

(2) $T_{bh} = T_b(I - Q)$ (Horizontally Polarized Brightness Temperature)

(3) $\boldsymbol{PD = T_{bv} - T_{bh}}$ **(Polarization Difference)**

- Range of PDs for 220 GHz calculated from all possible cirrus cloud cases are very small compared to the PD range for 680 GHz.
- Very compacted IWP and D_{eff} isolines among cases with D_{eff} < 80 μm regardless of IWP value indicating very low PD sensitivity for 220 GHz and 680 GHz.
- Ignoring the range of PDs for 220 GHz, there is high sensitivity for cases with IWP > 60 gm^{-2} and D_{eff} > 80 μm as the isolines become separated enough to become distinguishable.
- Numerical PD signatures indicated that PD for 680 GHz was increasing for increasing D_{eff}.
  - Appears to approach a maximum when D_{eff} gets to 100 μm.
  - Trend is similar to results in a study done by J. Miao et al. (2003).
    - As D_{eff} increased from 0 μm, PD signatures increased until a maximum was approached at a certain D_{eff} at each frequency.
    - Magnitude of the maximum PD increased while the corresponding D_{eff} decreased going from small to large frequencies.
- Frequencies larger than 220 GHz needed to likely observe high sensitivity among the selected IWPs and D_{eff}s for this study

Sub-mm/mm Brightness Temperature Depression (ΔT_b) Sensitivity

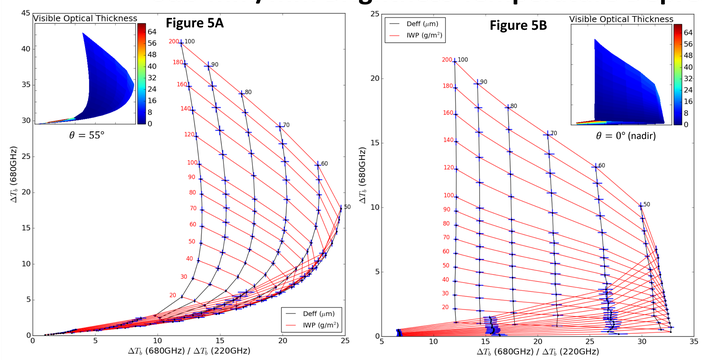

Figure 5A and 5B: IWP (red) and D_{eff} (black) isoline plots with respect to ΔT_b (680 GHz) and ΔT_b (680 GHz) / ΔT_b (220 GHz). The potential error lines (blue) are centered at all intercepts of the IWP and D_{eff} isolines which represent a cirrus cloud case. The visible optical thickness (τ) contour subplot contains axes of the same scale as the main plot. The viewing zenith angle (θ) for Figure 5A is 55°. The viewing zenith angle (θ) for Figure 5B is at nadir.

$\Delta T_b = T_{bclearsky} - T_b$ **(Brightness Temperature Depression)**

- Figures 5A and 5B show a clearer visualization of how sensitive 680 GHz and 220 GHz are to IWP and D_{eff} compared to Figure 4.
- Similar to Figure 4, both frequencies appear to be sensitive to the larger ends of the IWP and D_{eff} ranges.
- **Figure 5A:**
  - IWP and D_{eff} isolines begin to separate for D_{eff} > 50 μm due to 680 GHz being sensitive to these particle sizes.
  - Range of IWPs that 680 GHz and 220 GHz are sensitive to increases as D_{eff} increases from 50 μm.
  - The ΔT_b (680 GHz) / ΔT_b (220 GHz) ratio first increases then decreases as D_{eff} values go from 10 μm to 100 μm.
    - 220 GHz appears to be sensitive to D_{eff}s > 50 μm while 680 GHz is sensitive to D_{eff}s smaller than this.
- **Figure 5B:**
  - Isolines are structured similarly to what is seen in Figure 5A.
  - D_{eff} isolines are nearly perpendicular to the x-axis (ΔT_b (680 GHz) / ΔT_b (220 GHz) ratio).
  - θ at nadir reveals that the ΔT_b (680 GHz) / ΔT_b (220 GHz) ratio is sensitive to all D_{eff} values.
    - The overlap in isolines are likely due to the ratio not being composed of adjacent frequencies (Evans and Stephens, 1995).
- Decent sensitivities to all IWPs and D_{eff}s would likely require frequencies greater than and adjacent to 680 GHz.

IR Brightness Temperature Difference (BTD) Sensitivity

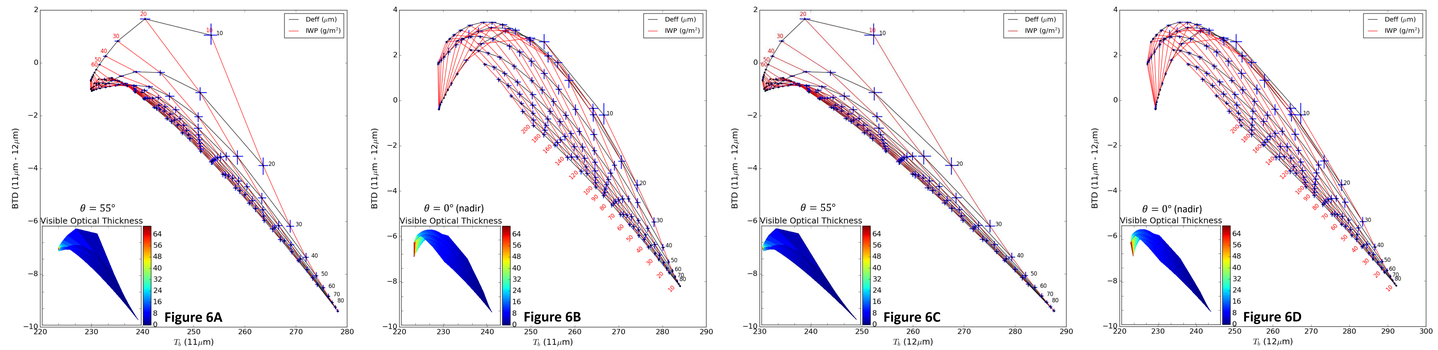

Figure 6A and 6B: IWP (red) and D_{eff} (black) isoline plots of BTDs with respect to 11 μm-12 μm BTD and 11 μm T_b. The potential error lines (blue) are centered at all intercepts of the IWP and D_{eff} isolines which represent a cirrus cloud case. The visible optical thickness (τ) contour subplot contains axes of the same scale as the main plot. The viewing zenith angle (θ) for Figure 6A is 55°. The viewing zenith angle for Figure 6B is at nadir.

Figure 6C and 6D: IWP (red) and D_{eff} (black) isoline plots of BTDs with respect to 11 μm-12 μm BTD and 12 μm T_b. The potential error lines (blue) are centered at all intercepts of the IWP and D_{eff} isolines which represent a cirrus cloud case. The visible optical thickness (τ) contour subplot contains axes of the same scale as the main plot. The viewing zenith angle (θ) for Figure 6C is 55°. The viewing zenith angle for Figure 6D is at nadir.

- The set of IWP and D_{eff} isoline plots (Figures 6A-6D, 7A-7D) were inspired by the series of τ and D_{eff} isoline plots created by Wang et al. (2011) using the same BTDs.
- 11 μm–12 μm BTD is known as the "split-window" technique.
  - 11 μm is a "clean" window IR channel as there is very little absorption of energy by water vapor.
  - 12 μm is a "dirty" window IR channels as there is a moderate absorption of energy by water vapor.
  - Positive 11 μm–12 μm BTDs are typically indicative of thin, semitransparent cirrus.
  - Negative 11 μm–12 μm BTDs are typically indicative of ash/dust clouds.
- **Figures 6A – 6D (11 μm–12 μm BTDs):**
  - At $\theta = 55°$ (Figures 6A and 6C), BTDs are sensitive to cirrus cloud cases with IWP < 60 gm^{-2} and D_{eff} < 20 μm.
    - Values correspond to what is typically found in thin cirrus.
    - 11 μm–12 μm BTD sensitivity to the lower ends of the IWP and D_{eff} ranges in contrast to sub-mm/mm PD and ΔT_b sensitivity to the higher ends.
    - Cases with large IWP and D_{eff} values have largely negative BTDs which are indicative of ash/dust clouds rather than cirrus clouds.
  - θ at nadir (Figures 6B and 6D), all IWP and D_{eff} isolines are compacted.
    - General insensitivity to both IWP and D_{eff} for 11 μm and 12 μm.
    - Similar trend to the $\theta = 55°$ situation in which small IWP and D_{eff} cases generally had positive BTDs while large IWP and D_{eff} cases generally had negative BTDs.

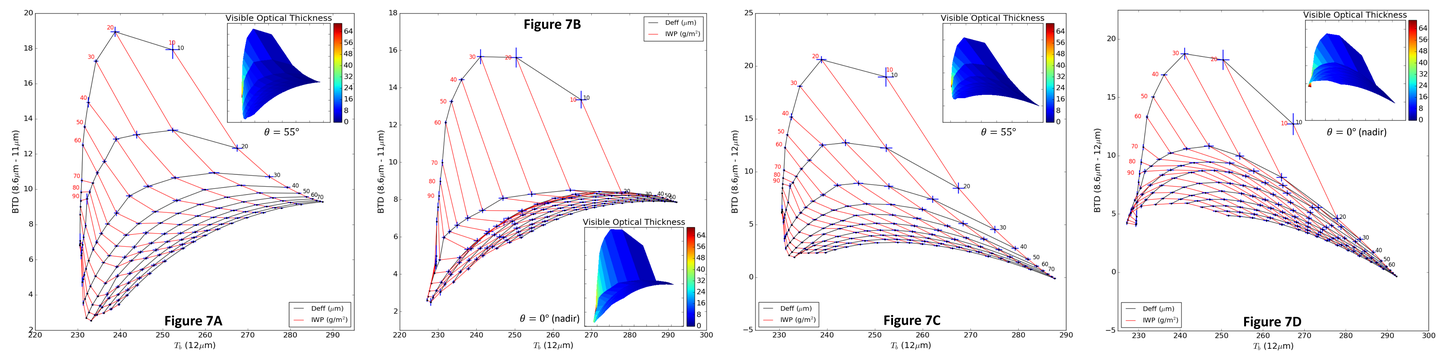

Figure 7A and 7B: IWP (red) and D_{eff} (black) isoline plots of BTDs with respect to 8.6 μm-11 μm BTD and 12 μm T_b. The potential error lines (blue) are centered at all intercepts of the IWP and D_{eff} isolines which represent a cirrus cloud case. The visible optical thickness (τ) contour subplot contains axes of the same scale as the main plot. The viewing zenith angle (θ) for Figure 7A is 55°. The viewing zenith angle for Figure 7B is at nadir.

Figure 7C and 7D: IWP (red) and D_{eff} (black) isoline plots of BTDs with respect to 8.6 μm-12 μm BTD and 12 μm T_b. The potential error lines (blue) are centered at all intercepts of the IWP and D_{eff} isolines which represent a cirrus cloud case. The visible optical thickness (τ) contour subplot contains axes of the same scale as the main plot. The viewing zenith angle (θ) for Figure 7C is 55°. The viewing zenith angle for Figure 7D is at nadir.

- 8.6 μm has been used in conjunction with 11 μm and 12 μm to infer cloud phase and type (e.g. Mixed Phase, Thick Ice, Thin Ice) (Menzel et al. 2004).
  - 8.6 μm is known as the "cloud top phase" band.
  - Positive 8.6 μm–11 μm and 8.6 μm–12 μm BTDs are indicative of ice clouds.
  - Negative 8.6 μm–11 μm and 8.6 μm–12 μm BTDs are indicative of water clouds.
- **Figures 7A and 7B (8.6 μm–11 μm BTDs):**
  - At $\theta = 55°$ (Figure 7A), BTDs are sensitive to a larger range of cirrus cloud cases than 11 μm–12 μm BTDs.
    - Decent BTD sensitivity for cases with IWP < 90 gm^{-2} and D_{eff} < 50 μm.
    - BTD magnitude and sensitivity greatest for cases with IWP < 60 gm^{-2} and D_{eff} < 20 μm (thin cirrus).
  - θ at nadir (Figure 7B), nearly all IWP and D_{eff} isolines are compacted.
    - BTD very sensitive to cases with IWP < 90 gm^{-2} and D_{eff} < 20 μm.
    - Both IWP and D_{eff} isolines are compact for cirrus cloud cases with D_{eff} > 20 μm regardless of IWP value indicating insensitivity.
- **Figures 7C and 7D (8.6 μm–12 μm BTDs):**
  - At $\theta = 55°$ (Figure 7C), BTDs are sensitive to a smaller range of D_{eff}s than the 8.6 μm–11 μm BTDs.
    - BTDs still remain sensitive to the smaller end of the IWP and D_{eff} values (IWP < 90 gm^{-2}, D_{eff} < 40 μm).
  - θ at nadir (Figure 7D), a similar trend to Figure 7B is present with nearly all IWP and D_{eff} isolines being compacted.
    - Somewhat less BTD sensitivity to cases with IWP < 90 gm^{-2} and D_{eff} < 20 μm compared to Figure 7B (8.6 μm–11 μm BTD, θ at nadir) indicated by less D_{eff} isoline separation.

IWP and D_{eff} Sensitivity Isoline Plots

- The IWP and D_{eff} isoline plots involves the measurement of brightness temperature parameters for different wavelengths at the x- and y-axis.
- Cirrus cloud cases calculated in ARTS are plotted in a way to create lines of constant IWPs and D_{eff}s (isolines) with each intercept representing a specific case.
- Degree of separation between the IWP and D_{eff} will determine how sensitive the wavelengths are to changes in these parameters.
  - Largely separated isolines will indicate high IWP or D_{eff} sensitivity (optimal for retrievals).
  - Compacted isolines will indicate low IWP or D_{eff} sensitivity (unfavorable for retrievals).
- Potential error calculations for each case were done by a 4 sub-pixel assumption (Merrellie et al.2012).
- A visible optical thickness (τ) contour subplot is also included with each IWP and D_{eff} isoline plot.
  - X- and y-axis still have the same ranges as those of the isoline plot.
  - τ not considered for an isoline plot due to IWP/D_{eff} ratio being the same among certain cases (Figure 3).
    - $\tau = \frac{3}{2}\frac{IWP(Q_e)}{\rho_i D_{eff}} = 3 * \frac{IWP}{\rho_i D_{eff}}$ (Visible Optical Thickness, Extinction Coefficient $\langle Q_e \rangle \approx 2$)

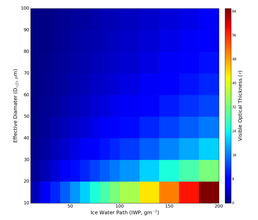

Figure 3: Visible optical thickness grid with respect to the IWPs and D_{eff}s selected for this study.

Summary and Conclusions

- 680 GHz PDs are moderately sensitive to the majority selected ranges of IWPs and D_{eff}s based on the PD range (x-axis) shown on Figure 4.
  - 220 GHz generally insensitive to all cirrus cloud cases based on the extremely small PD range (y-axis).
- 680 GHz and 220 GHz ΔT_b and ΔT_b ratio provide decent sensitivity for a larger range of IWP and D_{eff} values compared to PD calculations.
  - 680 GHz ΔT_b sensitive to larger ends of the IWP and D_{eff} ranges (IWP > 20 gm^{-2}, D_{eff} > 50 μm).
  - When θ at nadir, IWP and D_{eff} isolines are neatly organized and could be useful for retrieval of IWP, D_{eff}, and τ.
  - With increasing D_{eff}, ΔT_b ratio initially increases then decreases as 220 GHz is sensitive to cases with large D_{eff}.
- **Sub-mm/mm frequencies higher than and/or adjacent to 680 GHz needed to make PD and ΔT_b useful for IWP, D_{eff}, and τ retrievals.**
- 11 μm–12 μm BTD (split-window technique) sensitive to a small amount of cirrus cloud cases when $\theta = 55°$.
  - Sensitive to cases with the smallest IWPs and D_{eff}s (IWP < 60 gm^{-2}, D_{eff} < 20 μm).
  - BTDs are largely negative for cases with D_{eff} > 30 μm which are usually indicative of ash/dust clouds instead of cirrus.
- 8.6 μm–11 μm and 8.6 μm–12 μm BTDs are sensitive to cases with IWP < 90 gm^{-2} and D_{eff} < 40 μm when $\theta = 55°$.
  - The 8.6 μm–11 μm and 8.6 μm–12 μm BTDs remain above 0 for all cases which indicates the presence of ice clouds.
  - When θ at nadir, sensitivity increases only for very thin cirrus cloud cases (IWP < 90 gm^{-2}, D_{eff} < 20 μm).
- **IWP and D_{eff} isoline plots using the wavelengths from both sub-mm/mm and IR regions can be useful to observe decent sensitivity for all cirrus cloud cases and be able to retrieve IWP, D_{eff}, and τ.**

Acknowledgements

- Thank you to Adam Bell and Guanglin Tang for providing ARTS control files and codes that made doing the ARTS calculations possible.
- This project is supported by the grant awarded by NASA's Earth Sciences Division (ESD) as part of the project entitled: "SWIRP: Compact Submm-Wave and LWIR Polarimeters for Cirrus Ice Properties" under the Instrument Incubator Program (IIP).

References

Buehler, S., C. Emde, P. Eriksson, O. Lemke, 2017: Atmospheric Radiative Transfer Simulator (ARTS) User Guide.

Emde, C., S. A. Buehler, C. Davis, P. Eriksson, T. R. Sreerekha, and C. Teichmann, 2004: A polarized discrete ordinate scattering model for simulations of limb and nadir longwave measurements in 1D/3D spherical atmospheres. *Journal of Geophysical Research*, **109**, .

Evans, K. F., and G. L. Stephens, 1995b: Microwave Radiative Transfer through Clouds Composed of Realistically Shaped Ice Crystals. Part II: Remote Sensing of Ice Clouds. *Journal of the Atmospheric Sciences*. **52**, 2041-2057.

Liu, G., J. A. Curry, 2000: Determination of Ice Water Path and Mass Median Particle Size Using Multichannel Microwave Measurements. *Journal of Applied Meteorology*. **39**, 1318-1329.

J. Miao, K.-P. Johnsen, S. Buehler, A. Kokhanovsky, 2003: The potential of polarization measurements from space at mm and sub-mm wavelengths or determining cirrus cloud parameters. *Atmospheric Chemistry and Physics*. **3**, 39-48.

Menzel, W. P., 2004: Chapter 6 – Detecting Clouds. *Applications with Meteorological Satellites*. 6-1 – 6-32.

Merrellie, A., 2012: The Atmospheric Information Content of Earth's Far Infrared Spectrum. *J. UWAOS*. **19**.

Prabhakara, C., R. S. Fraser, G. Dalu, M.-L. C. Wu, R. J. Curran, and T. Styles, 1988: Thin cirrus clouds: Seasonal distribution over oceans deduced from Nimbus-4 IRIS. *Journal of Applied Meteorology and Climatology*, **27**, 379–399.

Troitsky, A. V., A. M. Osharin, A. V. Korolev, J. W. Strapp, 2003: Polarization of Thermal Microwave Atmospheric Radiation Due to Scattering by Ice Particles in Clouds. *Journal of Atmospheric Science*. **60**, 1608-1620.

Wang, C., P. Yang, B. A. Baum, S. Platnick, A. K. Heidinger, Y. Hu, R. E. Holz, 2011: Retrieval of Ice Cloud Optical Thickness and Effective Particle Size Using a Fast Infrared Radiative Transfer Model. *Journal of Applied Meteorology and Climatology*. **50**, 2283-2297.